Available online at www.sciencedirect.com
SCIENCE DIRECT®
ELSEVIER
European Journal of Mechanics B/Fluids 23 (2004) 353–365
EUROPEAN JOURNAL OF MECHANICS B/FLUIDS

Experimental and computational study of square cylinder wakes with two-dimensional injection into the base flow region

Panayiotis Koutmos *, Demosthenes Papailiou, Andreas Bakrozis

Department of Mechanical Engineering and Aeronautics, University of Patras, Patras, Rio 26500, Greece

Received 26 February 2003; accepted 30 September 2003

Abstract

An experimental and computational investigation of unsteady turbulent wake flows past a two-dimensional square cylinder with planar jet injection from its base into the vortex formation region is presented and discussed. Detailed measurements of the mean and turbulent near wake development at a Reynolds number of 8520 and for various jet to approach flow velocity ratios were obtained with Laser Doppler Velocimetry to examine the aerodynamic performance of the wake flow under the complex jet/wake interaction arrangement. In the complementary computational work a Large Eddy Simulation procedure was employed to help analyze the rich variety of wake flow patterns that were identified in the experiments. Subgrid scale motions were modeled with a first-order closure utilizing an anisotropic subgrid eddy-viscosity and a prognostic equation for the subgrid scale turbulent kinetic energy. The detailed results help to evaluate the effects of base injection on the mean and turbulent characteristics of the near wake region while at the same time the performance of the computational model is appraised by comparing simulations with measurements for the range of the complex flow configurations studied here.

Keywords: Square cylinder wake; Vortex shedding flow; Large eddy simulation; Base injection; Large scale structure

1. Introduction

The time-varying turbulent flow field produced downstream of a two-dimensional bluff-body has frequently been considered as a model problem due to its fundamental importance in a physical sense as it encompasses the interactions among highly anisotropic regions, large scale recirculations, unstable shear layers and periodic or quasi-periodic energetic formation and shedding of vortices (Bearman [1], Williamson [2], Roshko [3]). Good understanding of the turbulent processes involved is necessary to improve methods of prediction (Rodi et al. [4], Breuer [5]) and allow better control or exploitation (Sreenivasan [6], Gad-el-Hak [7]) of these dynamic flow features in a wide range of engineering applications.

In the past several years insight into the basic physical aspects of the flow development in a generic bluff body configuration such as the square cylinder wake has significantly advanced as a result of intensive experimental and computational work (e.g., [1,4,8]) that provided detailed information within the near wake the main region of interest. In these investigations attention has focused on plane long two-dimensional square cylinders under confined or unconfined conditions due to the priority to exclude additional complexities and concentrate on the examination of the turbulent transport characteristics of the wake formation region.

An added complexity to this basic configuration is the injection of a low aspect ratio two-dimensional jet from the cylinder base along its symmetry plane into the wake base region. This flow/geometry combination (a set up that has also been referred

* Corresponding author.
E-mail address: koutmos@mech.upatras.gr (P. Koutmos).

0997-7546/$ – see front matter
doi:10.1016/j.euromechflu.2003.09.004

Nomenclature

C_{kij}	Sub-Grid-Scale (SGS) model constant
D, D_j	cylinder, fuel-jet height
k_s, k_r	SGS turbulence energy, resolved fluctuation energy
L_t	turbulence length scale
u, v	streamwise and cross-stream velocities
u_o, u_j	approach air-flow and jet injection velocities
S_{ij}, R	resolvable strain tensor, resolved fluctuations
x_i	Cartesian coordinate directions ($i = 1, 2$)

Greek symbols

δ_{ij}	Kronecker delta ($\delta_{ij} = 0$ for $i \neq j$, $\delta_{ij} = 1$ for $i = j$)
Δ, Δx, Δy	characteristic mesh sizes
ε_f	dissipation rate of scalar fluctuations
ρ, ν_t	density, SGS eddy-viscosity coefficient
τ_k	Kolmogorov time-scale
τ_{ij}, σ_{ij}	stresses

Operators

$\ldots'$	turbulent (subgrid-scale) quantities
$\langle \tilde{\ldots} \rangle$	grid-scale quantities
$\langle \bar{\ldots} \rangle$	time-averaged values

Subscripts

i	$i = 1, 2$, Cartesian coordinates
i, j	tensor notation
s	subgrid scale
t	turbulent flow

to as 'base bleed', see for example Bearman [9]) is relevant to a range of diverse engineering applications (Wood [10]) ranging from aeronautics and marine hydrodynamics to flame stabilization in power generation devices. This device was originally investigated and exploited in relation to drag reduction efforts in blunt trailing edge aerofoil sections [9,10]. The benefits that result from this aerodynamic interference with the unsteady wake structure were studied in these applications in a fashion similar to the splitter plate studies of Bearman [1] and Unal and Rockwell [11]. More recently, in a somewhat broader sense, Amitay et al. [12] studied wake interference through synthetic surface jets in an effort to alter the aerodynamic performance of two-dimensional circular cylinders, Patnaik and Wei [13] injected angular momentum into the base region of square cylinders at low Reynolds number to suppress the wake instability, while Lu et al. [14] reported drag reduction and wake stabilization benefits from base bleeding in spheres. The effects of base bleed (or base injection) in the generic two-dimensional square cylinder configuration have not been studied previously in detail and also only a limited amount of information on the performance of this type of wake interference has been reported for the studied aerofoil type geometries. Additionally the potential value of the above setup or other variants of similar type within the context of an active or passive control flow device warrants further investigations into the details of these complex unsteady separated flows.

On the other hand the complexity of the injected jet/unsteady cylinder wake interaction system and the multiplicity of possible parametric flow variations makes the exploitation of CFD methods an attractive option in the overall methodology of identifying an optimum configuration for a given application. The overall successful prediction of several important design parameters such as Strouhal number, drag and lift coefficient and some global flow features reported recently for the basic configurations (e.g., [4,5]) supports the use of simulation tools as an adjunct to experiments.

The present work then describes the experimental and computational investigation of turbulent wake flows past a slender square cylinder under 19% confinement, with two-dimensional jet injection into the vortex formation region. Detailed Laser-Doppler Velocimetry measurements were obtained by Bakrozis [15] throughout the developing wake region at a Reynolds number of 8520 for a wide range of injection (bleed) ratios to quantify the interaction between the injected jet and the turbulent wake.

In the supplementary computational work the Large Eddy Simulation procedure of Koutmos et al. [16] and Papailiou et al. [17] is extended and applied to calculate the measured flows; subgrid scale motions are here modeled by using an anisotropic subgrid eddy-viscosity and one equation for the subgrid scale turbulent kinetic energy. Computations are performed for selected injected wakes and the results are discussed and compared against the experimental data to complement the description of the detailed flow features, assess the accuracy of the numerical procedure and evaluate the parametric effects of base injection on the wake aerodynamics.

2. Flow configuration and experimental details

The experimental facility and a sketch of the square cylinder model are shown in Fig. 1(a). The square cylinder model ($D = 8$ mm) was inserted into a 5 : 1 aspect ratio rectangular cross-section duct of dimensions (height × width) 42 × 252 mm producing an area blockage of 0.19. At the inlet (L_1), located $4.5D$ upstream, uniform axial velocity profiles were measured

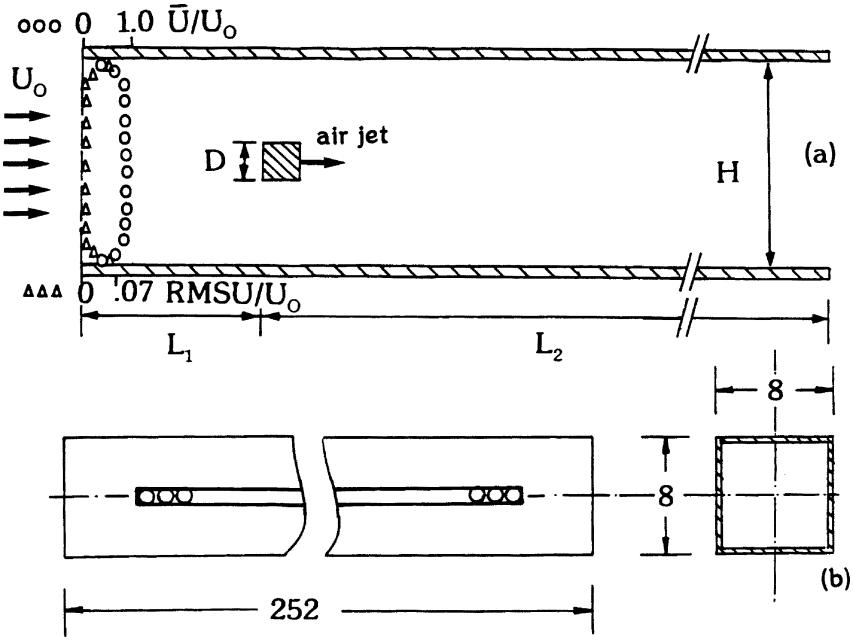

Fig. 1. (a) Wind tunnel geometry, flow configuration and inlet conditions. (b) Square cylinder model geometry and jet injection arrangement.

with Hot Wire Anemometry over 85% of the span with 0.1% turbulence levels ($\rho_{\text{air}} = 1.18$). The outlet of the measurement and computational domain (L_2) was placed at $27D$ downstream of the cylinder base and the origin of the streamwise axis x is on the cylinder base. Details of the rig and its operational characteristics may be found in Bakrozis [15].

The operating Reynolds number based on cylinder diameter and approach air velocity was 8520. Bleed air was fed through the cylinder ends and then injected into the base of the wake through 125 holes of 1 mm diameter closely spaced at 0.125 mm apart and lying on the horizontal symmetry plane (Fig. 1(b)). The spanwise uniformity of the injection was achieved by suitably tapering the hollow of the cylinder to adjust the injection pressure according to inviscid manifold theory. The discharge coefficient of each injection orifice was estimated at 0.62. LDV measurements suggested that this discrete jet system produced a spanwise planar jet within a distance of $0.25D$ when the cylinder was operated without crossflow, a distance that was even shorter when backflow was established. In the simulations the injection system was modeled as a spanwise slot of 1mm height maintaining the correct momentum efflux per unit span and allowing for increased bleed air inlet turbulence levels.

Transverse profiles of the time-averaged mean and turbulent streamwise and cross-stream velocities and related statistics were obtained throughout the wake with a single component Laser-Doppler Velocimeter consisting of a 2W A–I laser fiber-optics linked to standard TSI transmitting (TSI 9180A) and receiving optics (TSI 9160). The jet and the cross-flow air supplies were seeded separately with similar concentrations of dried powdered MgO particles dispersed by two purpose-built cyclone separators to minimize bias errors due to unequal particle number densities. The filtered Doppler signals were processed by a frequency (TSI 1980B) counter interfaced with a 32-bit computer. Mean and statistical values were derived by post-processing a sample of 20480 data. The data were weighted by the time between particles to correct for velocity bias effects due to random particle arrival times. Velocity fluctuation spectra were obtained by sampling the data at 4 kHz. Unormalized spectra were produced by a Fast Fourier Transform performed on 20 sets of 1024 values. Maximum uncertainties in the velocities due to non-turbulent Doppler broadening, sample size (statistical error) and sampling bias are less than 6% in the mean and less than 12% in the RMS. Extreme deviations due to seeding were determined by seeding only one of each of the two streams. The primary air stagnation position was unaffected while the jet stagnation position varied by 5%; the mean and RMS velocity values were similarly checked and found to change by 10% and 4% of u_o respectively in the vicinity of the cylinder base. Further details of the experimental method may be found in Bakrozis [15].

3. Numerical method

3.1. The formulation

The model description derives from the formulations adopted in Koutmos et al. [16] and Papailiou et al. [17]. Within the LES formalism each flow variable, e.g., velocity u is decomposed into the large (grid) scale velocity and the subgrid-scale

fluctuations u', i.e., $u = \tilde{u} + u'$. The classical box filter applied to the incompressible Navier–Stokes equations yields the equations describing the 'resolvable' flow quantities:

$$\frac{\partial \tilde{u}_j}{\partial x_j} = 0, \qquad \frac{\partial \tilde{u}_i}{\partial t} + \frac{\partial}{\partial x_j}(\tilde{u}_i \tilde{u}_j) = -\frac{1}{\rho}\frac{\partial \tilde{p}}{\partial x_i} + \frac{\partial}{\partial x_j}[2\nu \widetilde{S}_{ij} + \tau_{ij} + L_{ij} + C_{ij}], \tag{1}$$

where

$$L_{ij} = \tilde{u}_i \tilde{u}_j - \tilde{u}_i \tilde{u}_j, \qquad C_{ij} = \tilde{u}_i u'_j + u'_j u_j,$$
$$\tau_{ij} = -\rho u'_i u'_j, \quad \text{and} \quad \widetilde{S}_{ij} = \frac{1}{2}\left(\frac{\partial \tilde{u}_i}{\partial x_j} + \frac{\partial \tilde{u}_j}{\partial x_i}\right) \tag{2}$$

are the Leonard stresses, Cross terms, the subgrid (SGS) stresses and the Grid-Scale (GS) strain tensor. The Leonard and Cross terms are neglected within the context of the finite-volume scheme used here [17]. The SGS stresses are modeled as:

$$\tau_{ij} = -\bar{\rho}\overline{u'_i u'_j} = \mu_{t,ij}\left(\widetilde{S}_{ij} - (2/3)\widetilde{S}_{kk}\delta_{ij}\right) - (2/3)\bar{\rho}\tilde{k}_s\delta_{ij}, \tag{3}$$

while the subgrid SGS energy, $k_{\mathrm{SGS}} = 1/2u'_k u'_k$, is evaluated from a prognostic model equation of the form (Schumann [18]):

$$\frac{\partial \bar{\rho}\tilde{k}_s}{\partial t} + \frac{\partial(\bar{\rho}\tilde{u}_j\tilde{k}_s)}{\partial x_j} = \frac{\partial}{\partial x_j}\left[\left(\frac{\mu}{\sigma_k} + \frac{\mu_{tjj}}{\sigma_k}\right)\frac{\partial \tilde{k}_s}{\partial x_j}\right] - \bar{\rho}\overline{u'_i u'_j}\frac{\partial \tilde{u}_i}{\partial x_j} - \bar{\rho}C_\varepsilon\frac{\tilde{k}_s^{3/2}}{L_t}(\sigma_k = 1.0). \tag{4}$$

Its explicit evaluation is motivated by high Reynolds number applications, density variable flows (Nieuwstadt [19]) and the use of coarse grids (Menon and Yeung [20]). The evaluation of the eddy viscosity through k_{SGS} in combination with the anisotropic coefficient is likely to allow greater flexibility than the Smagorinsky model as suggested by Papailiou et al. [17] and Sohankar et al. [21]. It is therefore necessary to establish the performance and behavior of such a model by simulating complex recirculating flows such as those studied here. The SGS eddy-viscosity could be evaluated from the SGS energy as: $\mu_t = \bar{\rho}C_k L_t\sqrt{\tilde{k}_s}$, with the SGS length scale given by $L_t = \Delta = \sqrt{\Delta x_i \Delta y_i}$ where Δ is the characteristic filter length (mesh size). As C_k has been reported to vary significantly in various simulations here we evaluated an anisotropic coefficient C_{kij} following the work of [22] who proposed to model the SGS fluctuations in proportion to the resolved stress tensor rather than the strain tensor. C_{kij} is therefore obtained from the expression:

$$C_{kij} = \frac{(\bar{k}_s/\bar{k}_r)\overline{R}_{ij} + (2/3)\delta_{ij}\bar{k}_s}{\Delta\sqrt{\overline{k_s}}(2\overline{S}_{ij} - (2/3)\overline{S}_{kk}\delta_{ij})} \tag{5}$$

with the constraint $0.05 \leqslant C_{kij} \leqslant 0.5$. S_{ij}, R_{ij} and k_r are the resolved strain, stresses and fluctuating energy and (–) denotes a statistical average. For a range of meshes and isothermal or reacting conditions this formulation has proven satisfactory [17]. Test runs showed that the variable C_k formulation outperformed the standard Smagorinsky model while it was somewhat inferior but much smoother and about 15 to 20% less expensive, despite the additional k_{SGS} equation, than a dynamically adjustable C_s procedure. Although a dynamic formulation could have been more appropriate, our ongoing research work to include the effects of backscatter and anisotropy through the use of a dynamic SGS kinetic energy equation formulation and the adequate experience and results obtained from the present model in related works, [17], led to its choice in the present simulations. Further discussion on the SGS model performance is given in the Results section.

The numerical method for solving the filtered Navier–Stokes equations is based on a finite-volume approach employing a staggered arrangement in grid space. The method follows from further development of the procedures used in Koutmos et al. [16] and Papailiou et al. [17]. The convective and viscous flux terms have been discretized by using the second order central differencing scheme. Due to the imposed restrictions in the resolution of the viscous sublayer in the practical high Reynolds number flows addressed here a second order semi-implicit predictor–corrector scheme is used for time integration. An Adams–Bashforth scheme is employed for the time-advancement of the momentum equations without the pressure term in the predictor step, while a Poisson equation is then solved by a conjugate gradient method with incomplete Cholesky preconditioning to obtain the pressure correction variable which is finally used to correct the previously calculated provisional velocity field in the corrector step. Further details of the numerical solution method may be found in references [16,17].

The predictor–corrector scheme used here has significant similarities with the fractional step procedure described in Peyret and Taylor [23]. The present numerical method is second order accurate in space and time at least for the velocities (Nieuwstadt et al. [19]). This should be seen in conjunction with the limitations of the projection method (for the pressure solution) to first order accuracy, as has been discussed by Peyret and Taylor [23]. In relation to these aspects a commonly recognized problem in LES is how to differentiate between the impact of the numerical discretization errors and the SGS model used. These doubts can be contained and, in part, addressed through careful refinement studies in mesh size and time-step, as discussed below,

and also by performing controlled computations with the available SGS models in an attempt to apportion their effectiveness. The performance of the employed SGS model with respect to the Smagorinsky and dynamic models is further discussed in the Results section with the help of the available computations.

3.2. Numerical details

The calculation domain for all runs extended from $4.5D$ upstream to $25D$ downstream of the cylinder. Three Cartesian meshes were used comprising $71 \times 51 \times 10$, $91 \times 71 \times 10$ and $121 \times 101 \times 20$ (x, y, z) grid points. The finer mesh improved by 22% the higher moments and by 14% the mean results in the near wake with respect to the coarser mesh; improvements between the second and the third mesh arrangements were smaller reaching levels of 12% and 4% respectively for the quoted results. Further grid refinement proved inefficient and time-consuming within the context of the LES procedure and therefore the finer mesh was employed for all presented computations. The mesh was generated with the aid of geometric series separately for the cylinder wake flanks, the vortex formation and development region and the redeveloping wake. The first grid node adjacent to the cylinder wall was placed at $y/D = 5 \times 10^{-3}$ ($y^+ \approx 0.12$). The non-slip boundary condition for the Grid-Scale velocity was applied for the cylinder walls with a Van Driest damping function to account for wall proximity. The channel walls were modeled through the conventional law of the wall (see references [18,19]).

Although every possible effort through test runs was made to exploit carefully available grid lines in important flow regions, as one reviewer noted, the near wall treatment remains quite approximate in such simulations. It should also be added that, while the cylinder surface offers separation points fixed by the geometry and alleviates these difficulties to some extent, it is questionable whether the present resolution is adequate for the jet injection orifice region and the jet/cylinder backflow interaction region. The low aspect ratio injection arrangement used (jet/cylinder/channel height $= 1 : 8 : 42$) necessitated prohibitively high mesh resolution to appropriately resolve the near jet orifice region. Nevertheless, the present study investigates the developed LES technique, applies it as a concept in the simulation of engineering flow control applications involving a multiplicity of complex flow topologies and exploits it as an adjunct to the experimental efforts.

Inflow conditions for the Grid-Scale velocities were specified in accordance with the mean measured velocity profile taken at $4.5D$ upstream of the body while random fluctuations satisfying the constraints of incompressibility and measured u_{RMS} profile were superimposed on the mean velocities. For each simulation of successive injection ratios the results from the previous case were used as initial conditions for the next and this helped obtain significant savings in CPU times. At the outlet, the simple convective boundary condition:

$$\frac{\partial u_i}{\partial t} + c\frac{\partial u_i}{\partial x} = 0 \quad (c = \text{mean channel velocity}) \tag{6}$$

was implemented and found to work satisfactorily for the present simulations. Periodic boundary conditions were applied at the spanwise boundaries thus assuming quasi-two-dimensionality of the mean flow and statistical homogeneity in this direction. As a compromise between large spanwise extent and finer resolution near the cylinder the resolved span was chosen with a width of 4.5 cylinder diameters. A Neumann boundary condition was employed for the Poisson equation as discussed by Peyret and Taylor [23]. In the periodic spanwise direction $P'(x, y, z + W) = P'(x, y, z)$ was used. A time step of 5×10^{-5} sec was chosen. Flow statistics were computed over approximately $120(D/u_o)$ after an initial transient of about $60(D/u_o)$. Average values shown and discussed below were taken over time and the spanwise extent. Run times on a dedicated Pentium IV system were about 1.5 hrs per shedding cycle for the base case. The time-averaged total fluctuating (RMS) values were here obtained as:

$$u_{i,\mathrm{RMS}} = \sqrt{u^2_{i,\mathrm{RMS,GS}} + \frac{u^2_{i,\mathrm{RMS,GS}}}{0.5(u^2_{\mathrm{RMS}} + v^2_{\mathrm{RMS}} + w^2_{\mathrm{RMS}})}\, k_{\mathrm{SGS}}} \tag{7}$$

with $i = 1, 2, 3$.

4. Results

Both time-mean data and statistical quantities related to the development of the turbulent wake flows were measured for a range of injection ratios to examine the jet/wake interaction performance. Complementary LES results are also compared with the data to allow validation of the procedure and offer additional insight into aspects of the flows that were not measured comprehensively.

The overall flow development for each reported injection case is best portrayed with the help of the simulated time- and spanwise-averaged streakline plots shown in Fig. 2 together with the uninjected wake (Fig. 2, IR $= 0$). At the injection ratios of

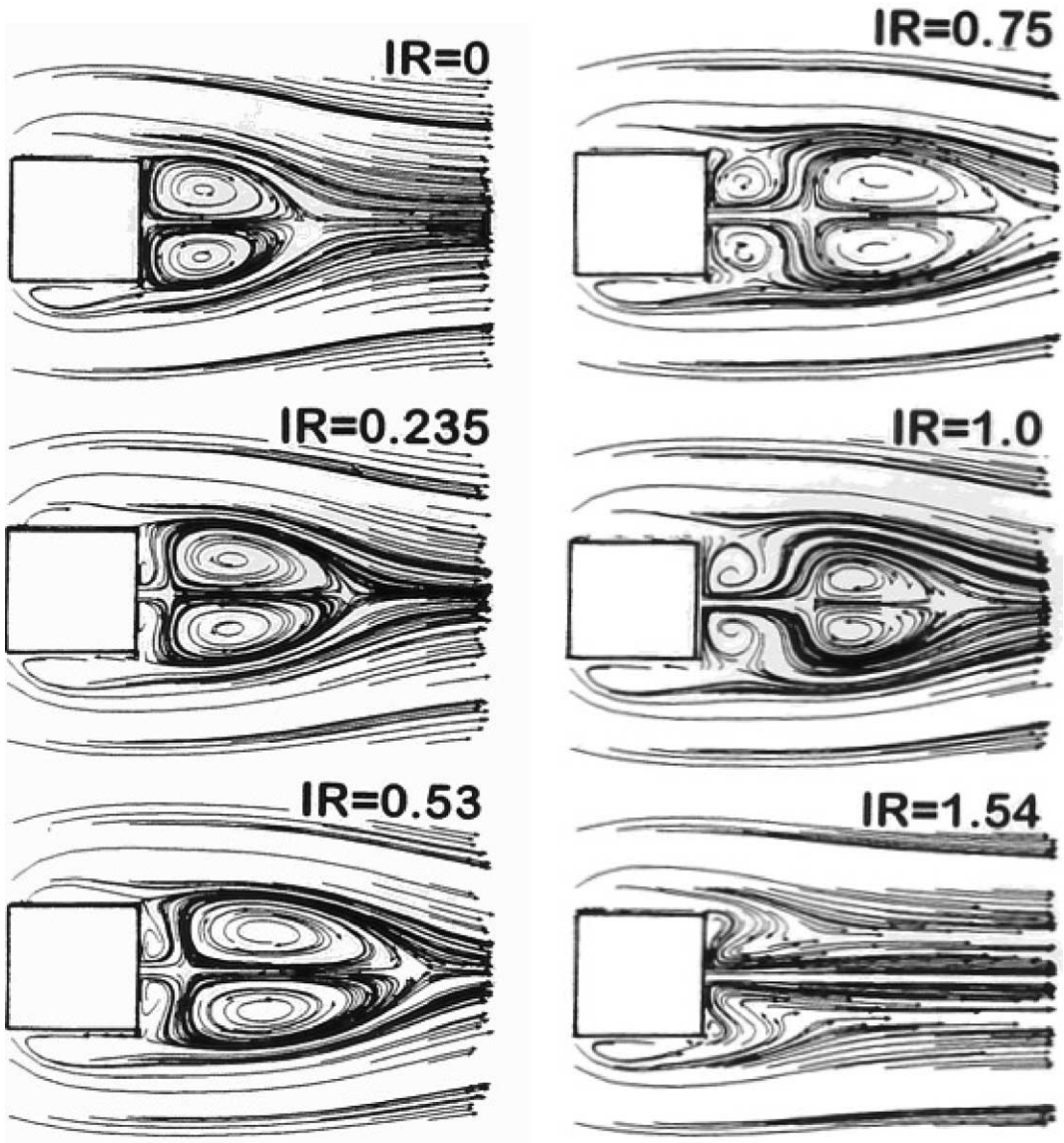

Fig. 2. Simulated time- and spanwise-averaged streakline plots for plane and injected wakes.

IR = 0.235, 0.53, 0.75 when the jet does not penetrate through the primary vortex, a system of four counter-rotating recirculation regions (two on each side of the symmetry plane) can be identified behind the cylinder occupying the wake formation region. The eddy centers and rotational directions are evident from these plots. These complex recirculating flow patterns depend on the balance between the dynamic pressures of the jet and the backflowing external air that creates the second stagnation position seen on the symmetry axis due to jet impingement and deflection. As primary air velocity increases (i.e., IR decreases) the air stagnation pressure increases and the aforementioned dynamic pressure balance is maintained closer to the cylinder base.

It is notable that with a 1.62% of mass injected ($m_{\text{injected}}/m_{\text{air}}$) at IR = 0.75 the primary recirculation lengthens and widens by 120% and 36% respectively by comparison to the plane wake. The reverse mass flow within the primary air recirculation, at IR of 0.235 and 0.53 suffers a moderate reduction and this may suggest that the formation region resists any change in its entraining capability at these lower injections. Only injections above about 0.60 begin to seriously affect the formation region entrainment ability with a reduction in the reverse mass flow of about 45% at a level of injection of 0.75. A different flow development emerges when, at the much higher IR of 1.54, the jet with increased momentum penetrates through the air recirculation. The overall flow pattern now resembles that of jet flow with two pairs of smaller vortices flanking the neck of the jet at the cylinder base. There was also a range of injection levels identified in the computations where a flow set up with a

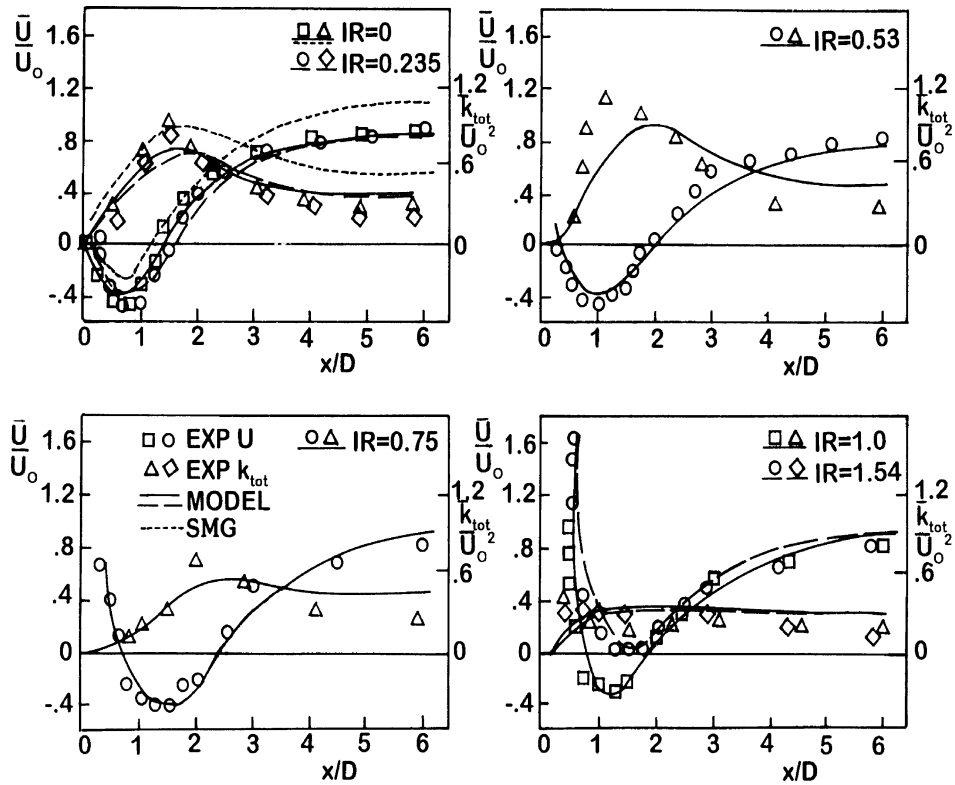

Fig. 3. Measured and calculated time-averaged streamwise velocity and total fluctuation energy distributions along the wake symmetry plane for various injection ratios (computations with present variable C_k formulation: —, – – –; Computations with the standard Smagorinsky (SMG) model (*comparisons are shown only for* IR = 0): · · · ·)

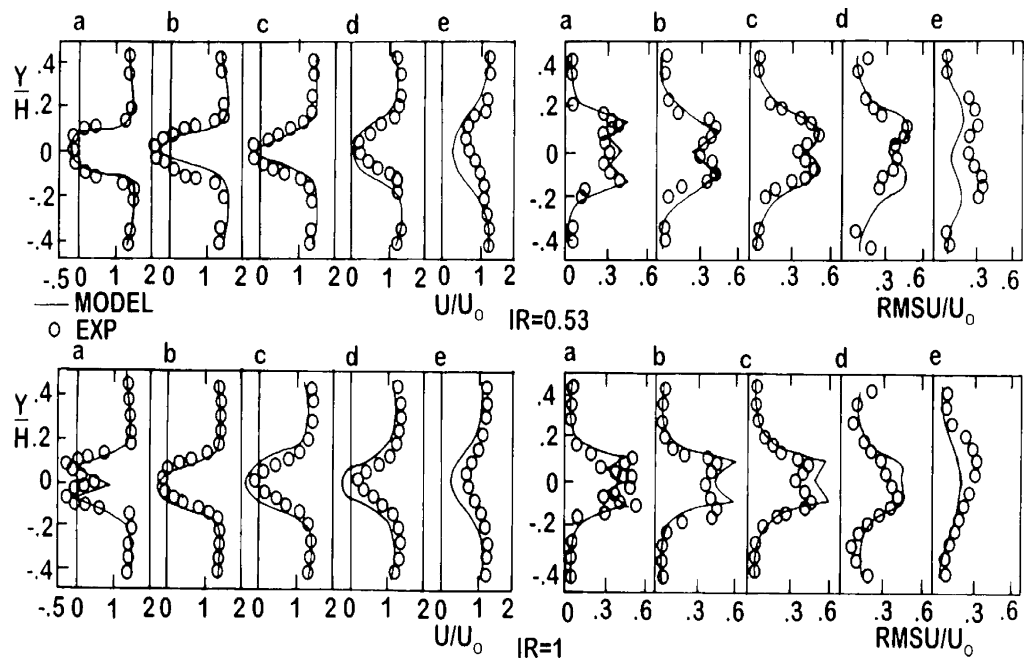

Fig. 4. Measured and predicted transverse distributions of time-averaged streamwise and cross-stream mean velocities and turbulence intensities for IR = 0.75 (stations a, b, c, d, e correspond to x/D positions of 0.5, 0.75, 1.0, 1.5, 2.25, respectively).

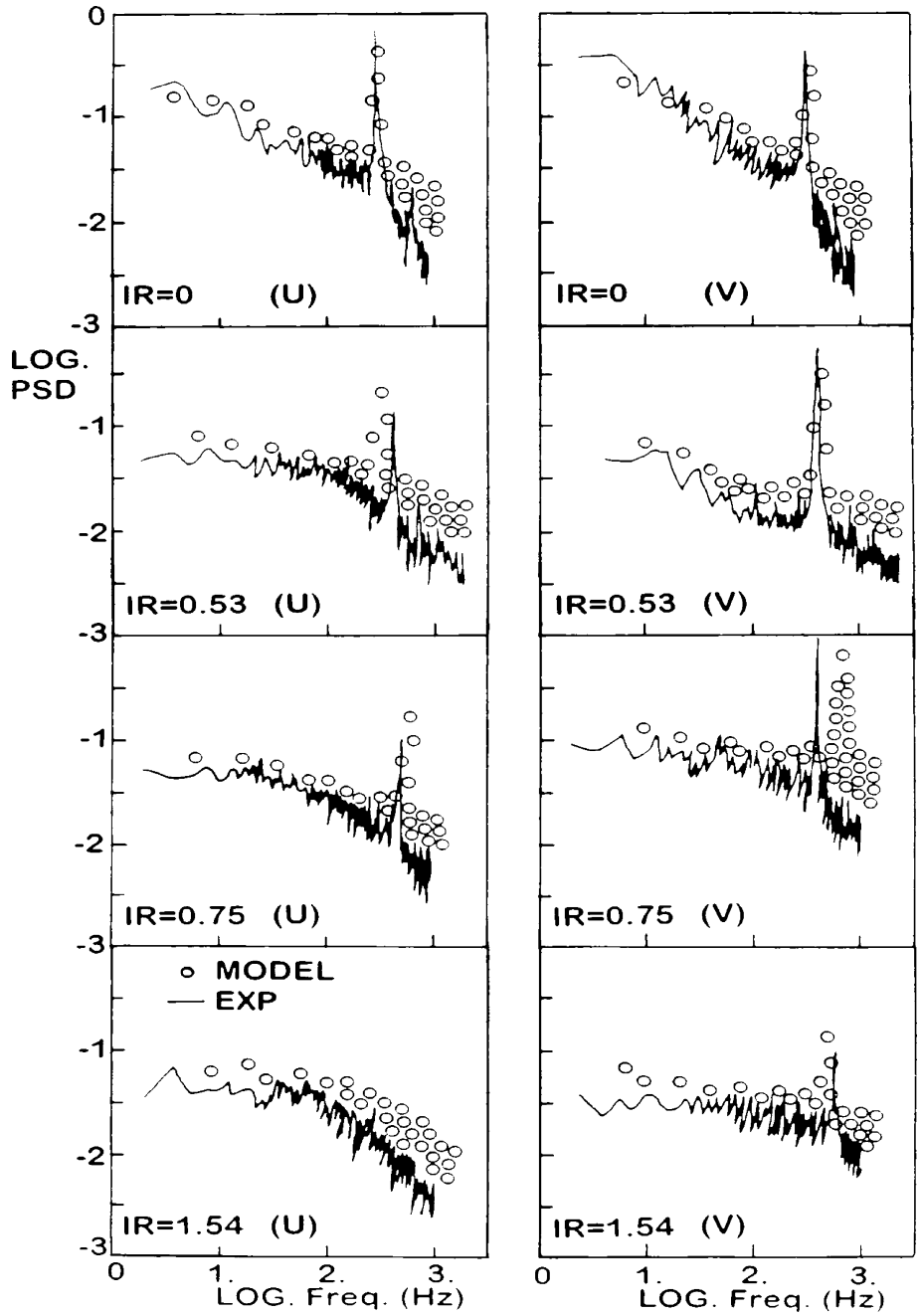

Fig. 5. Measured and predicted unormalised U and V velocity power spectra taken at $(x/D, y/D) = (3, 0)$ for various injection ratios.

system of six counter-rotating vortices was established within the near wake region as exemplified in the plot of Fig. 2 for IR of 1.0.

These pictures of the computational flow visualization correspond well to the detailed profiles measured throughout the near wake. Fig. 3 depicts the measured and calculated development of the time-mean axial velocity and total fluctuating energy (periodic + turbulent) along the symmetry plane for several injection ratios. Both simulated and measured energies include only the axial and normal intensities due to lack of measurements in the spanwise direction. The two stagnation points are clearly identified from the inflexion positions in these distributions (see also Fig. 2). Initially both stagnation points are pushed forward with injection ratio up to 0.6; as the jet gradually penetrates deeper the entrainment rate of the formation region is impaired and

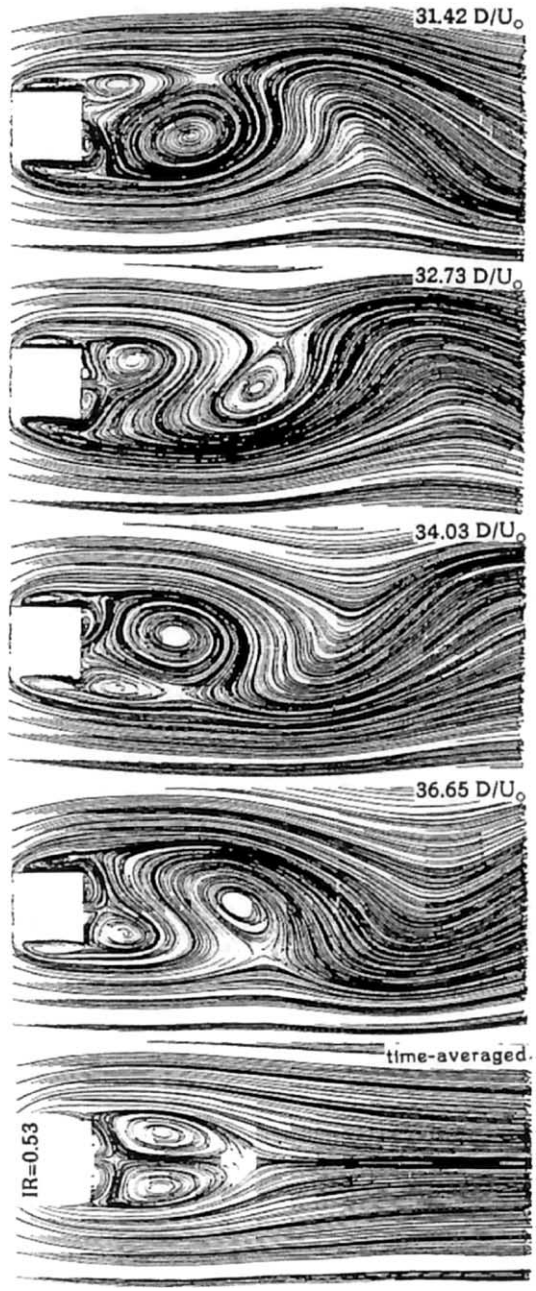

Fig. 6. Simulated streakline patterns for an injection ratio of 0.53 at successive flow times.

the above trend is reversed at about IR = 0.7 for the primary air stagnation point. Thereafter the strength and length of the main recirculation gradually diminishes until the dynamic head of the jet is sufficient to penetrate along the symmetry plane through the main recirculation at a IR of about 1.5.

A comparison between the performance of the standard (non-dynamic) Smagorinsky model and the variable C_k formulation is given in Fig. 3 (top left) for the plane uninjected wake case. The performance of the Smagorinsky model is similar to that reported previously (e.g., [16]) while the variable C_k model improves the agreement between experiment and simulation. Test runs with a dynamic Smagorinsky model somewhat improved predictions of mean values and first moments further, particularly as the grid was refined. These were however 15% computationally more expensive and required control of numerical instabilities, whilst the simpler variable C_k model gave smoother solutions. The present experimental data for the base line

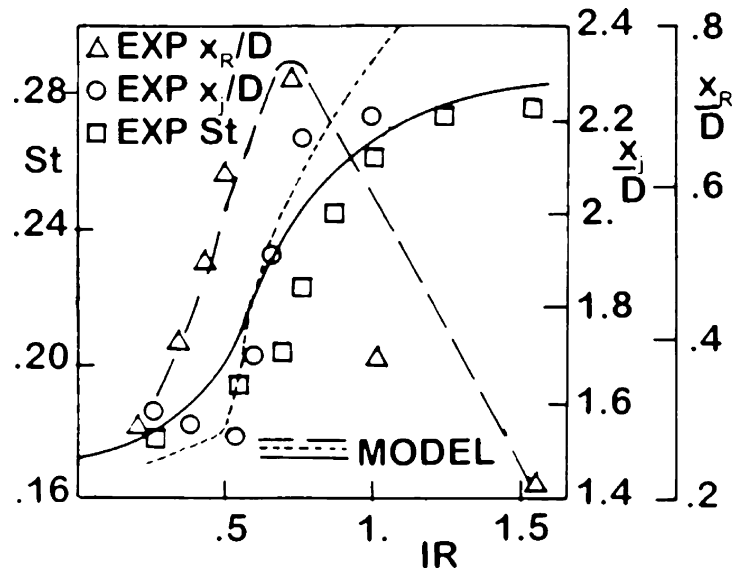

Fig. 7. Comparisons between measured and computed variations of the jet (x_j/D) and primary air (x_R/D) stagnation positions on the wake symmetry plane and Strouhal number (St) with increasing injection ratio.

uninjected wake can also be compared with the measurements reported by Lyn et al. [8] within the base and near wake region of a square cylinder operated at a Re = 22000 and a tunnel blockage of 7%. With respect to the global parameters, a higher Strouhal value of 0.176 was measured in the present configuration (St = 0.132 in reference [8]) while the predicted drag coefficient was 1.95 (2.13 in reference [8]). A mean recirculation length of $1.32D$, slightly shorter than $1.4D$ as reported in Lyn et al. [8], along with a much faster recovery of the mean and fluctuating fields were measured here due to the larger blockage of the present configuration. The maximum measured centerline value of the time-mean total fluctuating kinetic energy of 0.78 is higher than the value of 0.67 reported in [8] with the major contribution coming from the cross-stream component in both experiments. It is thought that the increased tunnel blockage effect leading to sharper shear layer gradients allows for augmented entrainment rates and compensates for the lower Reynolds number effects in the present square cylinder wake with respect to the wake development reported in Lyn et al. [8].

Detailed comparisons of the time-averaged transverse distributions of the streamwise and cross-stream velocities and intensities are given in Fig. 4 for a configuration in the unpenetrated (IR = 0.75) airflow dominated regime. Prior to penetration the effect of wake injection is to gradually reduce the levels of the transverse velocity, the main entraining component, due to the splitting effect of the jet in a fashion similar to a splitter plate (Bearman [9]). The entraining activity is then extended further away from the cylinder base and is, in part, replenished by the injection process. The replenishment increases with increasing injection and this aspect represents a crucial difference between splitter plate interference and the aerodynamic interference discussed here. Maximum RMS levels, located in the vicinity of the forward stagnation point, also vary accordingly. Peak turbulence generation results from the more energetic V component in the lower injection cases; as the jet penetrates further (IR > 0.53) the axial intensities are observed to increase gradually at the expense of the normal component. This trend is clearly corroborated from the successive k distributions of Fig. 3. Under full penetration the jet dissects the formation region and prevents the shear layers, emanating from the cylinder flanks, to interact. Any amplification of the initial instability is thus suppressed and not allowed to evolve into a regular vortex street. Again this behavior is somewhat similar to that seen in bluff-bodies fitted with splitter plates (Unal and Rockwell [11]). At higher IR turbulence generation occurs at off-axis positions for both the streamwise and the transverse components but peak levels are still lower than those found in the unpenetrated configurations since the periodic contributions are drastically diminished for IR greater than 1.0. This aspect should be seen in conjunction with the discussion of the periodic behavior of these wake flows following below.

Turning to the performance of the LES method the procedure has followed adequately the intense flow field variations occurring in the complex configurations simulated here in both the pre- and post-penetration regime. The time-averaged recirculation lengths were underestimated by 5 to 10% while the peak backflow velocities were underpredicted by 8 to 12% with the higher disagreement found in the near-penetration IR regime. The exact level of IR where jet penetration occurs was the most difficult to obtain accurately perhaps due to increased mesh requirements in the low aspect ratio jet injection arrangement used (jet/cylinder/channel height = 1 : 8 : 42) and it is believed that an even finer mesh would have been beneficial in delineating

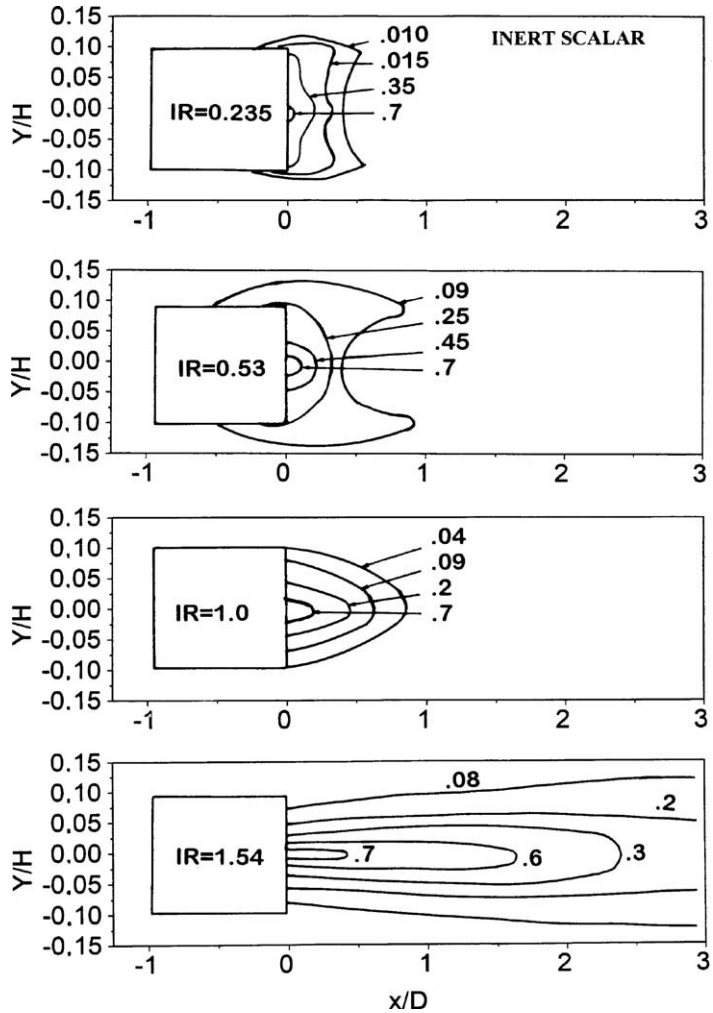

Fig. 8. Computed concentration contours for an inert scalar injected through the jet orifice at various injection velocity ratios.

the numerical inaccuracies involved therein. It is worth noting that discrepancies in the computed fluctuation levels increased as the periodic content in the total fluctuation energy was reduced with increasing IR.

The unsteady character of the jet/wake system is given in the form of the U and V velocity power spectra (Fig. 5) taken at $(x/D, y/D) = (3, 0)$ for successive IR. At low injection ratios the measured and predicted frequency peaks are well in line with the plane square cylinder shedding frequency corresponding to a Strouhal number of 0.176 with a 5 to 10% deviation for the simulations. It should be remarked that when the 'blocked' (factored by the appropriate area blockage) velocity passed the cylinder is used rather than the inlet approaching velocity the resulting Strouhal ($= 0.14$) agrees better with other literature values for lower blockages [1,8]. At higher IR, in the pre-penetration regime, the jet interferes more effectively with the basic vortex street producing a broader band of frequencies residing in the energy peak around a pronounced frequency. This peak gradually shifts towards higher values with increasing injection a trend also seen in the predicted spectra. This band of frequencies is thought to be connected to large and smaller scale vortices which are now irregularly shed, an observation that has been reported in previous studies (Bearman [9]) and for other forms of wake interference, e.g., splitter plates [1,11]. A transition to the post-penetration regime occurs at IR $= 1.5$ in the experiment and IR $= 1.45$ in the predictions although caution should be exercised for this predicted value since it was rather difficult to establish its exact level. The predicted and measured U spectra indicated that any periodic or quasi-periodic form of large scale vortex shedding was interrupted but in the V spectra a low energy peak still persisted in the middle wake region. A tentative explanation may be that the shear layers emanating from the cylinder flanks are prevented from interacting with each other due to the splitting effect of the jet. Vortex roll up still occurs however and develops along the streamwise direction adjacent to the jet flanks. Interaction is finally allowed (probably in a very weak sense) when far downstream the jet has mixed and lost its integrity. The measured and predicted remaining Strouhal is

about 0.27 a value that can be related to shear layer eddy formation. This behavior needs further clarification and its origin is currently under further experimental and numerical investigation.

The overall time-varying flow development with the alternating vortex shedding and the vortex street may be better inferred from the simulated streaklines at the middle plane for five sequential phases for an injection ratio of 0.53 shown in Fig. 6. The vortices formed on the bottom and top side walls of the cylinder are gradually intensified sliding round the corners and consecutively occupying the primary recirculation region. The process of vortex formation and shedding is displaced, with respect to the uninjected wake, further downstream from the cylinder base due to the effect of the injected jet, which apparently contributes to the formation process.

The measured and computed variation with injection ratio of three important performance parameters, i.e., the jet and primary air stagnation positions and the Strouhal number is depicted in Fig. 7. The initial rapid increase of the Strouhal number up to an injection of about 1.25 is followed by a plateau toward the last measured injection ratios. Beyond this IR value the regular shedding is curtailed giving place to the broader frequency distributions that appear only in the transverse component as discussed previously (Fig. 5). The Strouhal number trend shown in Fig. 7 is quite similar to that reported in the studies of Bearman [9]. If the present injection coefficient is transformed into the 'bleed coefficient' used in [9] (i.e., bleed coefficient $= [(C_D u_{\text{jet}} D_{\text{jet}}/(u_{\text{air,blocked}} D_{\text{cylinder}})])$ then the reported therein inflexion position where the Strouhal rise levels off is very close to the present IR value of 1.25. This signifies the very similar basic physical behavior of the present flow set up to the $2D$ aerofoil section with blunt trailing edge that was used in references [9] and [10]. A further notable future in the distributions of Fig. 7 is the similar trend in the variation of the jet stagnation position and the Strouhal number. The computational model has reproduced well the measured trends in these global parameters with the largest discrepancies identified in the predictions of the jet stagnation point as mentioned previously.

Since injection from struts is frequently exploited in a diversity of applications such as flame stabilization, ventilation, agriculture, the scalar mixing characteristics associated to the variety of complex flows described above are of practical significance. This can be studied most conveniently within the simulation model by computing the dispersion of a tracer released from the jet orifice. The inert scalar mixing contours thus obtained are shown in Fig. 8 for selected injection ratios. These expectedly reveal a rich variation of dispersive characteristics; the lower injection ratios maintain the released tracer within the near wake region at various extents and in some cases (e.g., IR $= 0.53$) even upstream of the cylinder base alongside its flanks while the higher injection ratios produce a jet-like mixing behavior releasing the tracer at further downstream distances.

5. Summary

Measurements and supplementary Large Eddy Simulations of the mean and turbulent wake flows created by a slender square cylinder with two-dimensional jet injection into the vortex formation region have been presented and discussed. Parametric studies of the effects of this type of base injection have been conducted for a range of jet to approach velocity ratios. At low injection ratios, prior to jet penetration through the primary vortex along the axis, a system of four or six counter-rotating recirculation regions was obtained within the formation region depending on injection ratio in both experiments and simulations. The overall wake recirculation length initially increases with injection but this trend is reversed at higher injections as the splitting effect of the jet gradually curtails the entraining capability of the formation region. With jet penetration the flow pattern resembles that of jet flow with two pairs of smaller secondary vortices flanking the neck of the jet at the base of the cylinder. The development of the periodic vortex street was observed to depend on the injection velocity maintaining its regular features at the initial stages of the jet/wake interference eventually breaking down and turning into irregular unsteadiness due to the splitting effect of the dissecting jet.

A variable SGS eddy-viscosity model was employed to simulate the range of flow configurations studied and produced improved results compared to the standard Smagorinsky formulation following well the complex variations identified in the experiments. Further detailed tests or refinements of the described methodology may be required to establish its usefulness and extend of its applicability. By translating the described passive aerodynamic jet/wake interference into an active interaction through the introduction of a suitable time-varying jet injection system (e.g., synthetic jet) it is likely that significant benefits may accrue depending on application. The exploitation of an accurate and reliable computational model may then prove a useful supplemental tool for a meaningful and convenient evaluation of the behavior of such variants of the basic flows studied here.

Acknowledgements

This work was partially funded by CEC contract JOUE-CT91-0077.

References

[1] P.W. Bearman, Vortex shedding from oscillating bluff bodies, Ann. Rev. Fluid Mech. 16 (1984) 195–222.
[2] C.H.K. Williamson, Vortex dynamics in the cylinder wake, Ann. Rev. Fluid Mech. 28 (1996) 477–539.
[3] A. Roshko, Perspectives on bluff-body aerodynamics, J. Wind Eng. Ind. Aero. 49 (1993) 75–100.
[4] W. Rodi, J.H. Ferziger, M. Breuer, M. Pourquie, Status of large eddy simulation: results of a workshop, J. Fluids Engrg. 119 (1997) 248–262.
[5] M. Breuer, A challenging test case for large eddy simulation: high Reynolds number circular cylinder flow, Int. J. Heat Fluid Flow 21 (2000) 648–654.
[6] K.R. Sreenivasan, Fluid turbulence, Rev. Mod. Phys. 71 (1999) s383–s385.
[7] M. Gad-el-Hak, Flow Control: Passive, Active and Reactive Flow Management, Cambridge University Press, London, 2000.
[8] D.A. Lyn, S. Einav, W. Rodi, J.H. Park, A laser-Doppler velocimetry study of ensemble-averaged characteristics of the turbulent near wake of a square cylinder, J. Fluid Mech. 304 (1995) 285–319.
[9] P.W. Bearman, Investigation into the effect of base bleed on the flow behind a 2D model with a blunt trailing edge, AGARD REPORT CP-4, 497, 1966.
[10] C.J. Wood, Visualization of an incompressible wake with base bleed, J. Fluid Mech. 29 (1967) 259–272.
[11] M.F. Unal, D. Rockwell, On vortex formation from a cylinder Part 2. Control by splitter-plate interference, J. Fluid Mech. 190 (1987) 513–529.
[12] M. Amitay, A. Honohan, M. Trautman, A. Glezer, Modification of the aerodynamic characteristics of bluff bodies using fluidic actuators, in: 28th AIAA Fluid Dynamics Conference, AIAA paper 97-2004, Snowmass Village, CO, June 29–July 2, 1997.
[13] B.S.V. Patnaik, G.W. Wei, Controlling wake turbulence, Phys. Rev. Lett. 88 (2002) 054502.
[14] M. Lu, F.R. Grosche, G.E.A. Meier, Drag reduction of a sphere at supercritical Reynolds numbers using passive ventilation, in: G.E.A. Meier, P.R. Viswanath (Eds.), IUTAM Symposium on Mechanics of Passive and Active Control, Kluwer Academic, Dordrecht, The Netherlands, 1999, pp. 127–132.
[15] A. Bakrozis, A study of turbulent diffusion flames stabilized by planar fuel jet injection into the wake formation region of slender square and round cylinders. Ph.D. Thesis, University of Patras, Patras, August 1997.
[16] P. Koutmos, C. Mavridis, D. Papailiou, A study of unsteady wake flows past a two-dimensional square cylinder with and without planar jet injection into the vortex formation region, Appl. Sci. Res. 55 (1996) 187–210.
[17] D. Papailiou, P. Koutmos, A. Bakrozis, Simulations of fuel injection and flame stabilization in the wake formation region of a slender cylinder, Proc. Combust. Inst. 28 (2000) 91–99.
[18] U. Schumann, Subgrid length scales for LES of stratified turbulence, Theor. Comp. Fluid Dyn. 2 (1991) 279–290.
[19] F.T.M. Nieuwstadt, R.J.M. Bastians, C.C.M. Rindt, A.A. Steenhoven, DNS and LES of transient buoyant plumes: a comparison with an experiment, in: D. Voke, L. Kleiser, J.P. Chollet (Eds.), Direct and Large Eddy Simulation I, Kluwer Academic, Dordrecht, The Netherlands, 1994, pp. 399–410.
[20] S. Menon, P.K. Yeung, Analysis of subgrid models using DNS and LES of isotropic turbulence, AGARD REPORT CP-551, 10, 1994.
[21] A. Sohankar, L. Davidson, C. Norberg, A dynamic one-equation subgrid model for simulation of flow around a square cylinder, in: 12th Australian Fluid Mechanics Conference, Sydney, Australia, December, 1995, pp. 517–520.
[22] T. Goutorbe, D. Laurence, V. Maupu, A priori tests of an SGS tensor model including anisotropy and backscatter effects, in: D. Voke, L. Kleiser, J.P. Chollet (Eds.), Direct and Large Eddy Simulation I, Kluwer Academic, Dordrecht, The Netherlands, 1994, pp. 121–131.
[23] R. Peyret, D. Taylor, Computational Methods for Fluid Flow, Springer-Verlag, 1985.